



# Influence of the Timber Shape on the Aerodynamics of a Timber Truck

Sadegh Fattahi, Petter Ekman, and Matts Karlsson Linköping University

**Citation:** Fattahi, S., Ekman, P., and Karlsson, M., "Influence of the Timber Shape on the Aerodynamics of a Timber Truck," SAE Technical Paper 2021-01-5045, 2021, doi:10.4271/2021-01-5045.

## Abstract

The aerodynamic improvement and efficiency of regular goods transportation trucks have been a topic of current interest; however, the timber transport industry has not been receiving as much attention. This is due to the small portion of timber transportation vehicles, compared to regular trucks, not justifying the cost of investigating these vehicles experimentally. Since these vehicles travel large parts of their journey at around 80 km/h, their fuel consumption is heavily affected by the aerodynamic resistance. In Sweden in 2015, there were around 2000 vehicles in operation transporting 6 billion ton-km with an average of 0.025 liter Diesel per ton-km. To understand these vehicles' aerodynamics, and improve on these in the future, the modeling of the timber stacks is of utmost importance.

Computational Fluid Dynamics (CFD) simulations have been utilized to conduct this investigation due to recent advancements and the relatively low cost of these simulations compared to an experimental approach. By investigating the influence of geometrical modifications of the stacks on the flow features and accumulated drag, a generic timber stack was created representative of a real stack for a loaded baseline vehicle. It was found that the shorter log length and a shuffling of the logs in the stack exhibit important flow features contributing to drag not present in the other cases. Based on this, a new baseline loaded truck configuration was created with all stacks being identical to each other. This generic stack was built with logs that were 4.25 m long and 0.35 m in diameter, had a smooth surface, and were stacked with a certain displacement in the lengthwise direction.

## Keywords

Timber, Truck, Aerodynamics, CFD, Computational fluid dynamics

## Introduction

Lowered fuel consumption and reduced greenhouse emissions of any type of road vehicles is an important challenge for the transport industry. For the transport industry, there has not been a focus as of yet, but a combination of environmental concern, fuel cost, and the fact the timber transport industry is an important link in a "green" value chain, this is about to change. As regular goods transportation trucks travel mostly at a speed of 80 km/h, the drag caused by aerodynamic resistance is responsible for around 25-50% of the fuel consumption, depending on road conditions, size, and weight of the vehicle [1]. Since fuel consumption is responsible for around 30% of the total operating cost, fuel efficiency is the main priority for timber-hauling companies [2]. In Sweden (2015) alone, there were about 2000 timber and chip vehicles in operation [3]. Every year these vehicles measure transporting six billion ton-km (metric ton-kilometers) with an average fuel consumption of 0.025 liter Diesel per ton-km [4]. Since these

timber transportation vehicles consist of components from different manufacturers, the vehicle as a whole is not in any way optimized for aerodynamic efficiency. Partially due to this, these trucks are not, as of now, fitted with any aerodynamic devices. Another reason for this is also the limited attention these trucks have been receiving within the field of aerodynamics. The aerodynamic drag of a fully loaded timber truck is responsible for around 20-30% of the fuel consumption per ton-km [5] and even higher when the truck is unloaded since no goods are being transported. One very important aspect of the fuel consumption for timber trucks is the fact that they only carry payload half of the distance and hence any appropriate aerodynamic reconfiguration must account for the loaded/unloaded case, respectively. Furthermore, several aspects, such as standstill time due to reconfiguration as well as cost and weight, are important aspects [5]. The loading of these vehicles is limited by the legal restriction for weight per axle; thus depending on the wood type and density variation

between the logs, each stack can be loaded to a certain extent. A lower density log will thus give the possibility of loading the truck with larger and/or more logs [6]. Due to this, the stacking of these trucks can differ depending on the type of timber. Even if the weight limits have not been exceeded, the individuals loading these trucks do not have knowledge about the effects of the stacking on the drag; thus they are not loaded in an efficient manner as regards to aerodynamics.

To reduce the effects of the aerodynamic drag, an understanding of the flow features around the whole vehicle is important. In the open literature, the availability of simulation and experimental data for timber trucks is very much limited, compared to regular trucks, where there exists a very extensive and wide range of conducted research [7, 8, 9, 10, 11]. With timber trucks travelling half of the time on the road unloaded, their aerodynamics need to be considered both in a loaded and unloaded case, which results in an aerodynamic performance of these vehicles that is much worse compared to a regular tractor-trailer vehicle benefiting from the same box-shaped exterior all the time that is not affected by their cargo. In addition, all timber logs have a different shape, size, and surface topology.

In this study modelling of the timber is investigated in detail using CFD to see how different stacks affect the aerodynamic performance of the timber truck. The stacks have been modified in surface roughness, length, diameter, shuffling of the logs, and different loading volumes on the same truck. This is performed for a yaw angle sweep from  $0^\circ$  to  $10^\circ$  with an increment of  $2.5^\circ$ .

Based on this, a new representative generic timber stack is created and used together with a realistic timber truck as a loaded baseline vehicle. As of now, there is no available literature on the modelling of timber nor the effect of the timber stacks on the aerodynamics of a timber truck. Thus this paper aims to present a baseline timber truck configuration currently not available, which can be used to gain a general insight into the flow features associated with these geometries and also be used for aerodynamic investigations and the improvement of the aerodynamic performance of the vehicles.

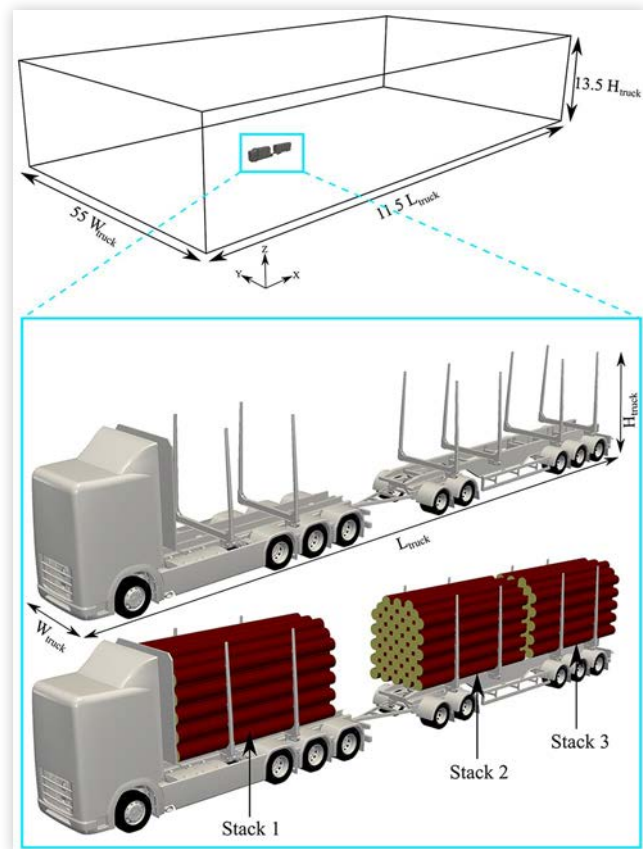
## Method

### Geometry and Computational Domain

The computational domain used for the timber study is presented in Figure 1, together with the simulated timber truck placed inside the domain. The truck used for this study is a 74-ton timber truck with a 1-3-2-3 axle configuration. The cab is simplified but includes the largest geometrical details such as the grill, cooler, and engine bay. However smaller geometrical entities and holes not affecting the flow field are removed.

The computational domain used for all the simulations is a rectangular domain with the dimensions of  $11.5$  vehicle length in  $x$ ,  $55$  vehicle widths in  $y$ , and  $13.5$  vehicle heights in  $z$ . The vehicle is placed in the domain with  $3.5$  vehicle lengths to the inlet. The vehicle dimensions are length  $L_{\text{truck}} = 23.71$  m, height  $H_{\text{truck}} = 4$  m, and width  $W_{\text{truck}} = 2.6$  m. The used

**FIGURE 1** Overview of the computational domain used for the timber study together with the geometry of the conceptual vehicle, in a loaded and unloaded case used for mesh sensitivity study with  $L_{\text{truck}} = 23.71$  m,  $H_{\text{truck}} = 4$  m, and  $W_{\text{truck}} = 2.6$  m.



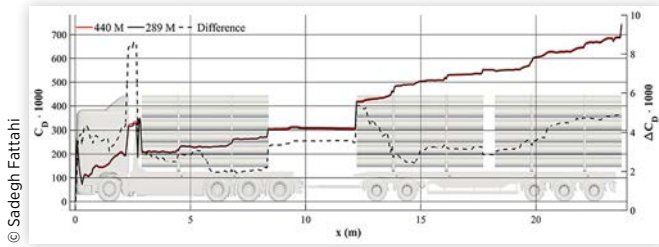
© Sadegh Fattahi

reference area is  $A = 10.4 \text{ m}^2$ , resulting in a solid blockage effect of  $0.15\%$ . The domain is compliant with SAE J2966 [12].

## Numerical Grid

The surface mesh is generated in ANSA v18.1.4 (BETA CAE Systems Sa., Thessaloniki, Greece) and consisting solely of triangular elements with a maximum skewness of  $0.5$ . The surface mesh consists of approximately  $23$  million triangular elements ranging between  $3 \text{ mm}$  and  $20 \text{ mm}$  in size. Surfaces such as the externals of the cab, timber, cooler inlet, wheels, A-pillar, and the stakes are meshed with the smaller elements while the underbody and the chassis are meshed with the largest elements. The volume mesh is generated in ANSYS Fluent 19.2 (Canonsburg, PA, USA), consisting of a Cartesian grid resulting in a mesh with a cell skewness of less than  $0.95$ . Inflation layers are generated on all of the truck surfaces and the ground. Depending on the level of exposure to the freestream flow, a different number of inflation layers are generated. At surfaces with high exposure such as the timber, wheels, cab exterior, banks, and stakes, six layers are generated with the first layer thickness of  $0.75 \text{ mm}$  and three layers for the rest of the surfaces of the truck such as the underbody with the first cell layer thickness set to give an aspect ratio of

**FIGURE 2** Drag for the two different mesh resolutions. A very small difference can be observed along the truck with a total difference of five drag counts.



six. At the ground, six layers are generated with the first cell height set to give an aspect ratio of eight. Two meshes are considered, the coarse mesh with 289 million elements and a fine mesh with 440 million elements. A comparison of the results, Figure 2, of the 440 million and 289 million domain shows that the 289 million mesh is sufficient, based on the accumulated drag along the vehicle, and is used for all the simulations. The difference in total drag between the two meshes is  $\Delta C_D = 0.005 \approx 0.5\%$ . The sensitivity studies are performed with the same model as in Figure 1, unloaded and loaded, and at a  $5^\circ$  yaw angle. The same meshing procedure is used for the unloaded case, resulting in a difference of the total drag between the two meshes of  $\Delta C_D = 0.009 \approx 1.1\%$ .

## Turbulence Modelling and Numerical Setup

In this investigation, the Realizable  $k-\epsilon$  (RKE) RANS turbulence model [13] is used together with an Enhanced Wall Treatment [14] with a  $y^+ \geq 30$ . This model has shown good agreement with experimental data performed for similar studies of external aerodynamics [15, 16, 17]. The pressure-based solver is used together with a coupled pressure-velocity scheme and a least-squares cell-based gradient scheme. The momentum and turbulent quantities ( $k$  and  $\epsilon$ ) are solved using second-order Upwind while the pressure is solved using the standard interpolation scheme. The standard scheme interpolates the pressure at the cell faces with the help of the momentum equation coefficients [14]. A pseudo-transient solver is utilized to reduce the computational cost. To reduce the computational cost, the simulation is first run with a high Courant number and increased underrelaxation factors for momentum and pressure. This is done to faster propagate the influence of boundary conditions into the domain. After that, the pseudo-transient solver is utilized with the highest possible pseudo time-step size before inducing instability in the solver. The pseudo time-step is then run till the residuals stop decreasing and then reduced by a factor of 2. The pseudo time-step reduction is performed until the drag forces stop fluctuating and converge to steady values with small fluctuations of 1 drag count.

All obtained data for post-processing are gathered and averaged over the last 200 iterations of the simulation to reduce small fluctuations in variables. A moving standard deviation of below 1 drag count of the last 200 iterations, for the drag coefficient, is accepted for post-processing to ensure convergence together with the residuals below  $10^{-4}$ .

All simulations are performed using ANSYS Fluent 19.2 at the Tetralith cluster at National Supercomputer Centre at Linköping University, Sweden ([www.nsc.liu.se](http://www.nsc.liu.se)). The computational cost on the Tetralith system is on average around 2000 CPU hours.

## Boundary Conditions

The inlet of the domain is set to a velocity inlet with a freestream velocity of  $U_\infty = 22.22 \text{ m/s} \approx 80 \text{ km/h}$ , a turbulent viscosity ratio of 50, and a turbulence intensity of 0.1%. The  $U_\infty$  used results in a width-based Reynolds number  $Re_{W\text{truck}} \approx 4$  million. The outlet of the domain is a pressure outlet with zero gauge pressure. The sides of the domain are set as symmetry for the  $0^\circ$  yaw case. For the cases with nonzero yaw angles, the right side, in the flow direction, is changed to a velocity inlet and the left side to a pressure outlet to mimic side wind conditions. Both velocity inlets are then modified by adding a  $y$ -component  $U_{y\infty}$  calculated according to Equation 1, where  $\beta$  is the yaw angle.

$$U_{y\infty} = U_\infty \tan \beta \quad \text{Eq. (1)}$$

The ground is set as a no-slip moving wall with the velocity  $U_\infty$ . The top of the domain is set as symmetry boundary conditions. The wheel rotation is replicated using a rotating no-slip wall with an angular velocity  $\omega$ . The cooling system is modelled using porous media to mimic the pressure drop across this region to account for added drag.

## Post-processing

The equations used for post-processing include the pressure coefficient (Equation 2), total pressure coefficient (Equation 3), and skin friction coefficient (Equation 4).

$$C_p = \frac{p}{0.5 \cdot \rho_\infty \cdot U_\infty^2} \quad \text{Eq. (2)}$$

$$C_{p\text{tot}} = \frac{p + (0.5 \cdot \rho \cdot U^2)}{0.5 \cdot \rho_\infty \cdot U_\infty^2} \quad \text{Eq. (3)}$$

$$C_f = \frac{\tau}{0.5 \cdot \rho_\infty \cdot U_\infty^2} \quad \text{Eq. (4)}$$

where  $p$  is the static pressure,  $\rho_\infty$  is the freestream air density,  $U_\infty$  is the reference freestream velocity,  $U$  is the local velocity magnitude,  $\rho$  is the local density, and  $\tau$  is the local wall shear stress. The wind averaged drag has been calculated for all cases according to SAE J5212 [18].

## Timber Geometry

The effects of the geometrical changes of the timber on the aerodynamic performance of the truck are studied to investigate important flow features and to create a generic timber stack to be used for the loaded baseline truck. The geometrical parameters of the timber investigated are surface roughness, length ( $L$ ), diameter ( $D$ ), and random shuffling of each of the

stacks, as well as increasing and decreasing loading volume from the first to third stack.

The length of a normal log can, in Sweden, vary between 3 m and 5.5 m and the diameter can vary between 0.12 m and 0.35 m [19]. Since all logs are not of the same length, a certain degree of shuffling of the stacks is present, meaning that the stacks do not have a perfectly flat face at the front or base.

Each modification of the timber will influence the flow field and gives rise to specific flow features, which in turn will affect the total drag, and to be able to compare these changes, a comparison is made to the stack in Figure 1, which will be referred to as the theoretical baseline stack. The theoretical baseline stack is based on the maximum length and diameter of a normal log, perfectly stacked timber with no protrusion of the logs and no surface roughness included. Each modification of the timber geometry is simulated for 0°, 2.5°, 5°, 7.5°, and 10° yaw except the surface roughness study, which is simulated for only a 5° yaw, which, according to a previous study, is the closest yaw angle to the wind averaged drag [19].

The surface roughness of the timber is modelled using Blender 2.80 (Blender Foundation, Amsterdam, The Netherlands) by connecting the movement of the nodes and setting this movement as random. By utilizing a sphere of influence larger than the stack, each node is moved in the normal direction of the surface by a distance of 10 mm or 20 mm for the two cases. The 10 mm and 20 mm movements of the nodes are combined with an STL element size of 32 mm and 64 mm, respectively. The stack used here is the same as the theoretical baseline stack as seen in Figure 3. The unevenness of the surface can be quantified, Figure 4, where the z-coordinates of the red line on the surface in Figure 3 are plotted along the timber.

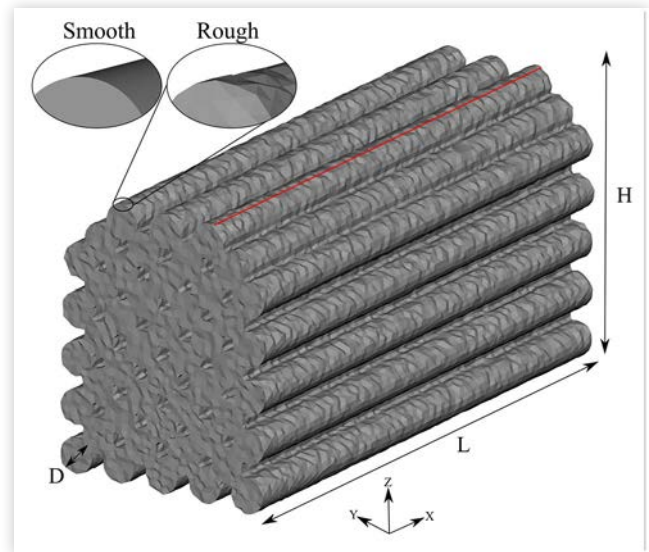
The lengths investigated are 3 m, 4.25 m, and 5.5 m, which correspond to the minimum, mean of minimum and maximum, and maximum. These lengths are combined with three different diameters of 0.12 m, 0.235 m, and 0.35 m corresponding to the minimum, mean of minimum and maximum, and maximum. The cases investigating the influence of the length and diameter of the logs are also simulated, with the voids between the logs being filled to investigate the effects of the voids on the aerodynamic performance and possible flow features associated with those.

Shuffling of the logs is made to give a more realistic stacking of the logs. The first shuffling of the stacks, Stacks 1 and 2 in Figure 5, is made using the same length and diameter for all the logs in the stack, thus only changing the position of each log along the x-axis of the truck. This is done with the max diameter and mean length of the logs.

A more randomized shuffling of the stacks is also performed by generating stacks with diameters and lengths ranging between the maximum and minimum values, Stacks 3 and 4.

Finally, two different cases are simulated where the loading volume and shuffling of each stack are unique. In this case, the second stack is similar in both cases; however, the positions of the first and third stack are swapped to get the increasing and decreasing loading volumes, which gives an increasing and decreasing stack height, from the first to the third stack. In the decreasing loading volume case, the stack with the largest volume is placed as the first stack and the

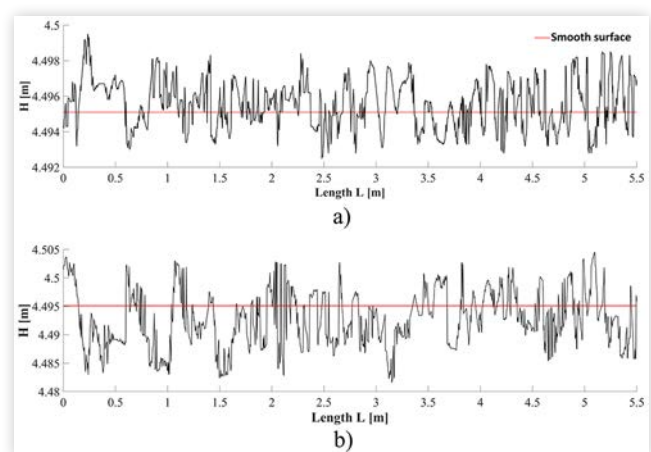
**FIGURE 3** The geometry of the timber stack used for the surface roughness investigation. The unevenness of the surface is modelled by moving the nodes of the STL geometry, referred to as rough. The red line indicates where the surface roughness plots are sampled in Figure 4.



© Sadegh Fattahi

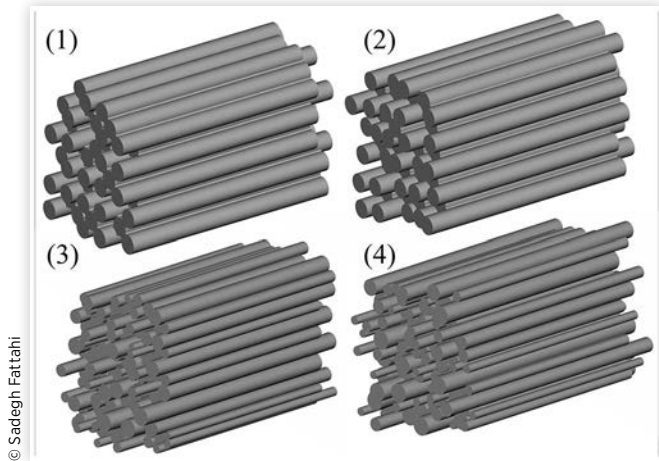
stack with the smallest volume as third, and vice versa for the increasing loading volume case. For the increasing loading volume case, the first stack is 21.9 m<sup>3</sup> and the second and third stacks are 5% and 12% larger than the first stack, respectively, giving an increasing loading volume starting from Stack 1. This also results in a front surface area of 4.71 m<sup>2</sup> for the first stack, and the front surface area of the second and third stacks are 6% and 15% larger than the first, respectively. The decreasing loading volume case has a reversed order of stacks, of loading volume and surface area, compared to the increasing loading volume case. All cases prior to that are simulated with

**FIGURE 4** The surface deviation along the z-axis of the red sample line in Figure 3 plotted along the length of the timber L for surface roughness of a) 10 mm and b) 20 mm. The red line shows the smooth surface with no variation. The 10 mm and 20 mm cases have a standard variation of 1.4 mm and 4.9 mm, respectively.



© Sadegh Fattahi

**FIGURE 5** The four different shuffled stacks created. In the top stacks, 1 and 2, the logs are only varied in the x-direction with same the diameter and length. The shuffled stacks with random length and diameter for each log can be seen at the bottom, 3 and 4.



all three stacks on the truck being copies of each other. The stacks used for these cases are Stacks 3 and 4 seen in [Figure 5](#), where few logs have been added or removed to get a larger or smaller loading volume.

A naming convention is used due to a large number of different stack designs. The parameters changing between the cases are length (L), diameter (D), shuffling (SH), and surface roughness (RS); thus the naming convention used will be as follows. For a case denoted L5.5\_D0.35\_RS0\_SH1, the first part refers to the length, in this case, 5.5 m; the second part to the diameter of the logs, 0.35 m; the third part to the surface roughness, in this case, smooth; and the last part to the shuffling of the stacks, in this case, shuffled Stack 1 seen in [Figure 5](#). A full list of the different parts can be seen in [Table 1](#), where a combination of these will be used to refer to each case.

**TABLE 1** The naming convention used to describe each stack, divided into four parts and each describing a certain feature of the logs.

First part	Second part	Third part	Fourth part
L5.5 = Log length of 5.5 m	D0.35 = Log diameter of 0.35 m	RS0 = Smooth surface	nSH = Not shuffled
L4.25 = Log length of 4.25 m	D0.235 = Log diameter of 0.235 m	RS10 = Rough surface 10 mm	SH1 = Shuffle 1
L3.0 = Log length of 3 m	D0.12 = Log diameter of 0.12 m	RS20 = Rough surface 20 mm	SH2 = Shuffle 2
L3.0-5.5 = Log length varying between 3 m and 5.5 m	D0.12-0.35 = Log diameter between 0.12 m and 0.35 m		SH3 = Shuffle 3
			SH4 = Shuffle 4

## Results and Discussion

The modelling of the timber in a loaded timber truck has an influence on the flow features occurring in the flow field, and they in turn have an influence on the drag of the truck. The extent of these effects is examined in this section, and a new generic stack is created based on the flow features associated with each stack configuration.

This section starts with an investigation of the influence of length and diameter of the logs, with nine different stack geometries, which are combinations of the three different lengths and diameters described in the method section. Later the same stacks, but with the voids between the stacks being filled, are investigated to examine if the voids are necessary to include or if they can be neglected. After that, the effects of shuffling, using the stacks seen in [Figure 5](#), are investigated to see if the protrusion of each log does affect the flow or if the stacks can be modelled as perfectly aligned at the front and base. Lastly, the importance of loading volume is investigated by removing or adding logs to the first and last stack, resulting in a difference in loading volume for each stack. This is done in an increasing and decreasing manner, meaning that the loading volume increases or decreases from the first to the last stack. Based on these results, a new generic stack is presented.

### Surface Roughness

The different stacks used in the surface roughness investigation are L5.5\_D0.35\_RS0\_nSH compared to L5.5\_D0.35\_RS10\_nSH and L5.5\_D0.35\_RS20\_nSH with two different surface roughness levels of 10 mm and 20 mm.

The 10 mm roughness stacks, [Figure 6](#), show no larger difference in any local region along the truck but rather a total accumulation along the entire truck leads to a higher overall drag count for the rough timber of about 8 counts ( $\Delta \approx 1.1\%$ ). Similar behavior is seen for the 20 mm roughness case but with a larger magnitude in the difference between smooth and rough, 14 counts ( $\Delta \approx 1.9\%$ ). The major difference starts at the front face of the second stack where the surfaces of the stacks are subjected to the freestream flow, unlike the first stack, which is mainly covered in the wake created by the separation from the deflector. A negligible change in friction

**FIGURE 6** The difference in total drag (solid line) and friction drag (dashed line) between the smooth and rough timbers along the truck. The differences, both total drag and friction drag, are larger for the 20 mm roughness case.

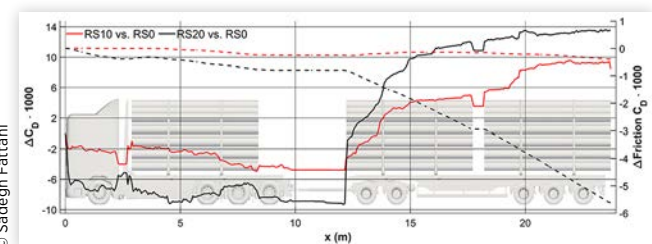
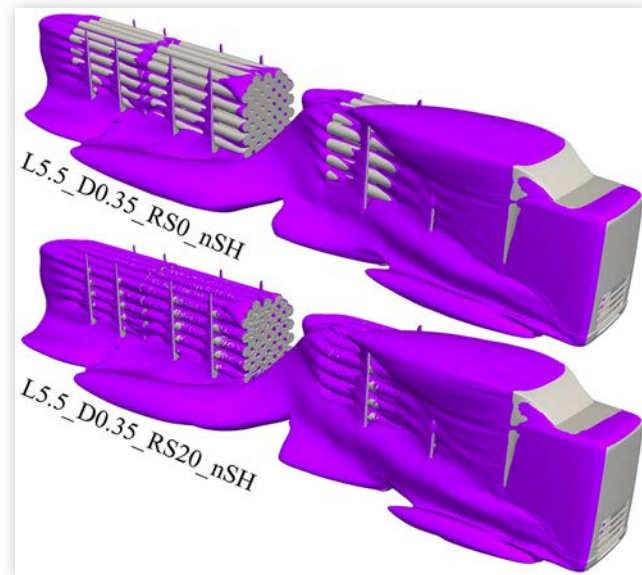


**FIGURE 7** Iso-surface of  $C_{p_{tot}} = 0$  for L5.5\_D0.35\_RS0\_nSH and L5.5\_D0.35\_RS20\_nSH at a 5° yaw. The only major difference between the cases is larger pressure loss regions at the surfaces of the stacks for the RS20 case while all other regions are almost identical.



drag is predicted for the 10 mm rough timber. The 20 mm case shows a larger difference in friction drag of  $-6$  counts.

The differences between the smooth and rough timbers are not mainly due to added friction drag but added pressure drag. This implies that the added drag is due to smaller wake structures along the timber, Figure 7, due to changes to the timber surface and area. This is especially noticeable from the start of the second stack. The results clearly indicate that the effects of using an uneven surface topology do not have a significant impact on the flow field or the drag. This uneven topology also yields a higher mesh requirement to be able to resolve the unevenness properly, thus resulting in an increased simulation cost.

## Length and Diameter

A summary of the influence of the diameter and length of the log on the drag, together with their wind averaged drag, can be seen in Figure 8. One trend between the cases is the decreasing wind averaged drag with increased log length. Another clear difference is the large decrease of wind averaged drag when the log length is 5.5 m for all three diameters, explained more thoroughly further on. It can also be seen that the wind averaged drag value is closest to the 5° yaw in all cases.

The 0° yaw cases do not follow the same trend as the cases simulated in a yawed condition. With increased yaw angle, the gaps will have a larger influence on the drag, but the 0° yaw is not influenced in the same manner since flow penetration between the gaps is not an issue to the same extent.

By comparing the drag for the different log diameters and the same length ( $L = 5.5$ ), Figure 9, the differences can be pinpointed. The major difference starts from the beginning of the second stack where  $D = 0.235$  m and  $D = 0.35$  m show the largest and the least drag, respectively. The reason for the

**FIGURE 8** The drag for length and diameter investigation. The black line represents the wind averaged result for each case. The wind averaged drag is decreasing with decreasing stack length for all three diameters investigated.

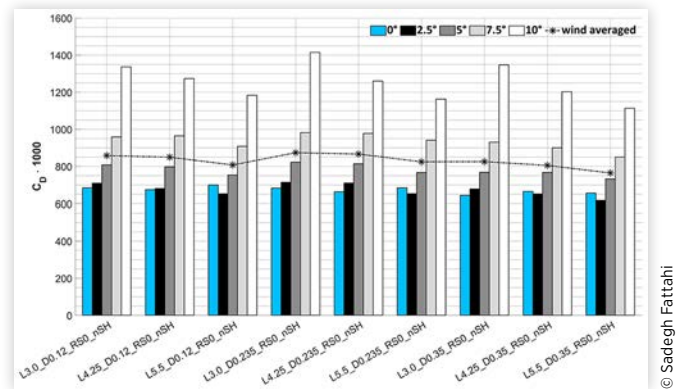
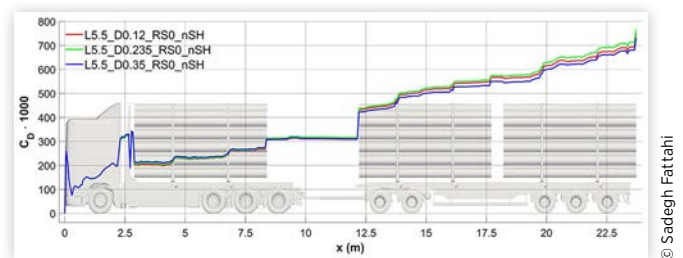


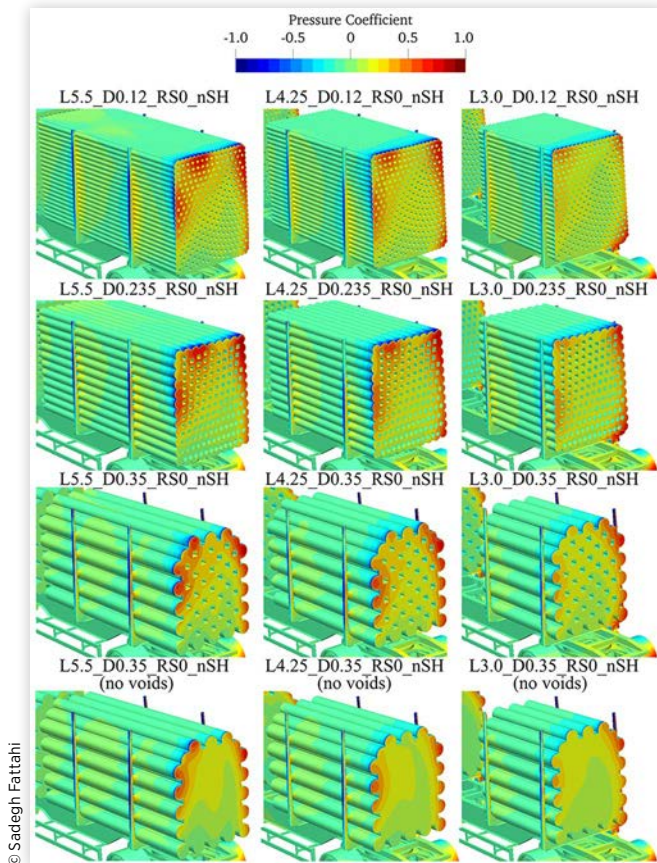
**FIGURE 9** Drag accumulation along the truck for  $L = 5.5$  m with different diameters at a 5° yaw.  $D = 0.235$  has the highest drag and stacks with  $D = 0.35$  have the lowest, with main differences starting at the front of the second stack.



lowest drag with the largest diameters is mainly due to the fact that with a larger diameter, the truck cannot be loaded to the same extent as for the smaller diameters, neglecting the possible weight limitations; thus the front and base surface area of the stack will be smaller, Figure 10, giving a lower pressure drag contribution. The pressure distribution at the front face of the stacks shows larger similarities between  $D = 0.12$  m and  $0.235$  m, showing larger areas of high pressure, especially at the top and sides. The largest drag for  $D = 0.235$  m is mainly due to the larger surface area of the front face of the stack. The larger surface area of the front face of the stack also consequently gives a smaller void area between the logs. Since there is a larger pressure difference between the front and base of each stack, these voids allow for high-energy flow to pass through and reduce these pressure differences, explained more thoroughly further on. Lastly, some of the increased drag for the case with  $D = 0.235$  m comes from the increased surface area inside the stack, contributing to added friction drag. Besides these factors, the change in diameter does not show any specific flow feature associated with a specific diameter.

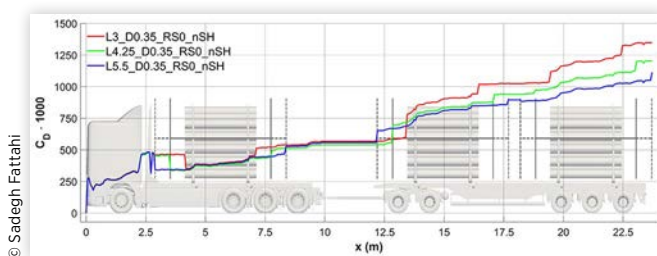
As expected, the drag decreases with increased log length, which is more noticeable with a higher yaw angle. By comparing the results for the three log lengths with  $D = 0.35$  at a 10° yaw, Figure 11, one can see the differences. The comparison is done at a 10° yaw since the effects of the log length are more pronounced but still showing the same trend

**FIGURE 10** Pressure coefficient of the second stack at a 5° yaw for all the different length and diameter configurations as well as the cases with filled voids for  $D = 0.35$ . The front surface area differs between the stacks depending on the diameter. The cases with  $D = 0.235$  have the largest front surface area and  $D = 0.35$  have the smallest. The location of the high-pressure regions on the front surface of the stack is consistent between the cases with the same length.



as the intermediate yaw angles. The drag along the truck does not differ noticeably, small differences can be seen in front of the bulkhead till the end of the first stack. Larger changes in the drag start just before the beginning of the second stack. Due to the increased distance between the first and second stack, with decreased log length, the size of the wake in that

**FIGURE 11** The drag for the three log lengths with  $D = 0.35$  at a 10° yaw. The dashed line and solid line in the background show the start and end of the stacks with  $L = 5.5$  and  $L = 4.25$ , respectively, together with the background picture showing the short stack.



area also increases, which gives rise to a low-pressure zone, which is most noticeable between the longest and shortest stack length. This particular behavior of increased drag due to increased gap size between the stacks is in agreement with track tests performed, studying the effects of the timber length on the fuel consumption [20].

From the beginning of the second stack till the base of the vehicle, the longest log length has a more gradual increase in drag compared to the shorter log lengths with a steeper curve.

A flow feature present for the short log length is the high-energy flow finding its way between the first and second as well as second and third stack, Figure 12, giving rise to larger stagnation regions on the front face of the stacks, Figure 13. Here the windward side of the stacks has a much larger surface pressure due to the high-energy flow finding its way in between the gaps. The flow entrainment between the stacks, especially between the second and third stack, is predominant with all log lengths except at  $L = 5.5$  m, Figure 12. Here the y-velocity is larger in front of the third stack for the shorter logs. This flow entrainment contributes to a large pressure drag at the front surfaces of these stacks. This can be seen as a sudden increase in drag at  $x = 19$ – $20$  m (depending on the stack length), Figure 11, with the largest increase for  $L = 3.0$  m. The longer logs make the wake of the truck start further downstream compared to the shorter logs, which also leads to this region containing less of the high-energy flow. Due to this, the high-energy flow is more deflected around the sides of the dolly, for the longer logs, which gives a larger pressure on the third axle of the trailer. For the shorter logs, the flow is more

**FIGURE 12** Left: The normalized y-velocity, red towards the plane, at the centerline of the truck ( $y = 0$ ) at a 10° yaw. Right: The total pressure coefficient at a yz-plane located downstream of the third stack, as shown with the dashed line in the left figure. With stack lengths  $L = 3.0$  m and 4.25 m, flow entrainment is more pronounced between the second and third stack as well as the first and second stack compared to  $L = 5.5$  m. Lower pressure regions are present at the leeward side (left) of the stack for the shorter log lengths.

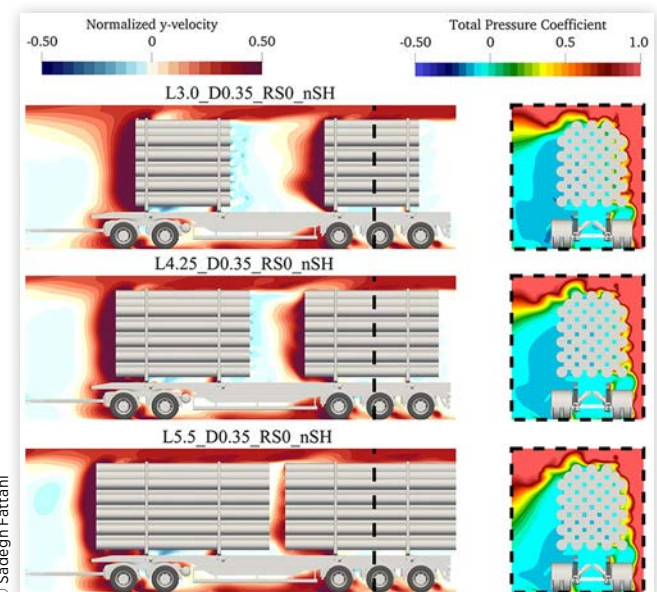
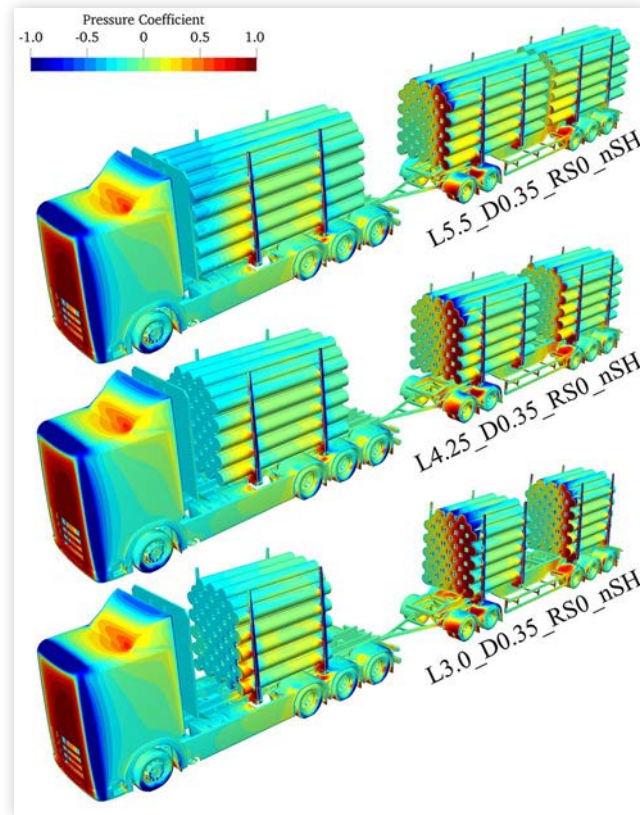


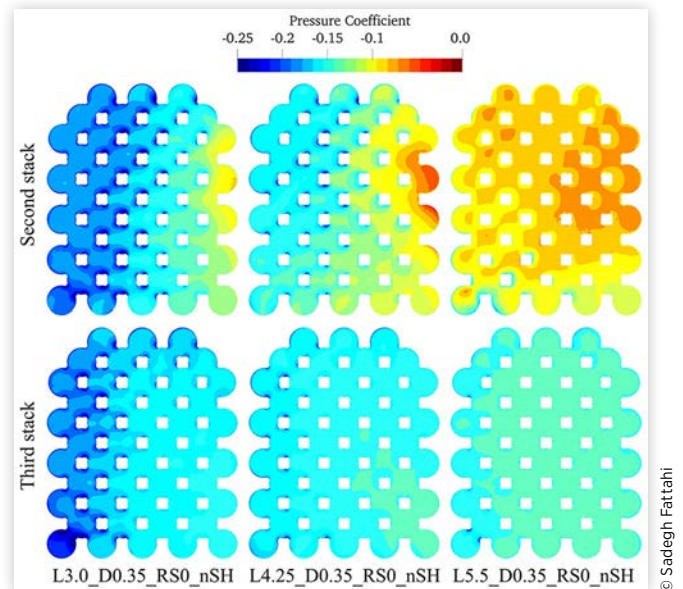
**FIGURE 13** Pressure coefficient for three different log lengths with  $D = 0.35$  at a  $10^\circ$  yaw. The most noticeable differences between the cases are the large increase in pressure on the face of the second and third stack with the decreasing log length.



directed downwards towards the underbody of the dolly and increasing the surface pressure on those regions.

At the base of the second stack, Figure 14, a larger low-pressure region is present with a reduced log length. This is due to the formation of a vortical structure between the stacks redirecting the high-energy flow from the windward side to the leeward side, resulting in lower pressure on the windward side. The increased drag due to the formation of a larger low-pressure region between the second and third stack is due to the fact that the distance between the stacks is large, which is not the case for  $L = 5.5$  m. The contribution of the low-pressure region can clearly be seen in Figure 11, where the drag suddenly increases for  $L = 3.0$  and  $4.25$  at  $x = 16$ – $17$  m (depending on the stack length) at the base of the second stack, not occurring for  $L = 5.5$  m. A similar behavior is observed with length variation for the other two diameters. The longer log lengths, which reduce the flow entrainment between the second and third stack, instead redirect the flow towards the underbody of the vehicle as well as the stakes. This results in a higher pressure on the underbody surfaces and slightly increased wake behind the stakes. Moving further down at the base of the third stack, Figure 14, a similar pattern can be seen with lower pressure with decreased log length and also the low-pressure region concentrated on the windward side. Based on these results the change in diameter does not show any flow features associated

**FIGURE 14** Pressure coefficient of the base of the second and third stack at a  $10^\circ$  yaw. The shorter log length has a much lower pressure at the second stack, but the differences reduce between the lengths at the base of the third stack.

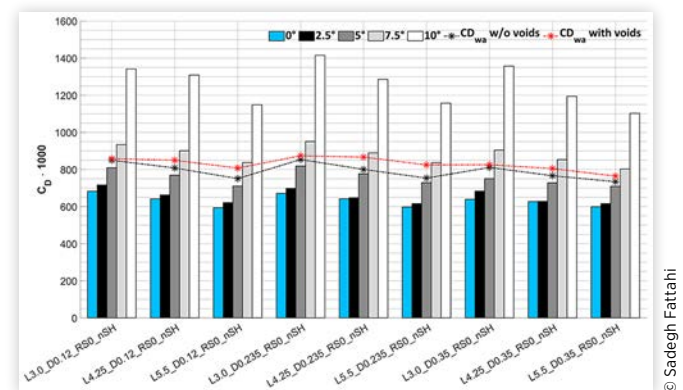


with a specific size; however, the length of the logs significantly impacts the flow field and the vehicle drag.

## Voids

The cases with filled voids between the logs generally show the same drag trend as that of the cases with voids, where the shorter log lengths show larger total drag. It also shows a drag reduction for the majority of the cases, compared to the cases with voids, and the wind averaged drag is lower for all cases without voids, Figure 8 and Figure 15. A small fraction of the reduced drag is because filling these voids does reduce the

**FIGURE 15** The drag for the same cases as in the length and diameter investigation but without any voids between the logs. The black and red lines represent the wind averaged drag without and with voids, respectively. The wind averaged drag is decreasing with decreasing stack length for all three diameters investigated and is lower for all cases compared to the stacks with voids shown in Figure 8.



friction drag due to a reduced surface area inside the stacks. However, the major contribution to the reduced drag is because filling these voids reduces high-energy flow entrainment between the first and second stack.

The different levels of flow entrainment are due to these voids acting as suction regions sucking the high-energy flow through the voids to even out the pressure difference between the front and base of the stack. This effect is less dominant with longer log lengths since the high-energy flow has a much lower tendency to enter between the first and second stack compared to the shorter log lengths, due to the gap distance between the stacks being smaller. The effects are seen looking at the total pressure at a vertical plane in the middle of the vehicle, ( $y = 0$ ) for L4.25\_D0.35\_RS0\_nSH at a 5° yaw, Figure 16, as the total pressure at the front face of the second stack is larger for the case with the voids. The case with the voids also has a slightly higher total pressure in front of the first stack since these voids even out some of the pressure differences. As seen in the same figure, the direction of the flow through the voids between the logs is different for the three stacks. The first stack has a negative flow direction along the x-axis while the other two stacks have a positive flow direction with a larger magnitude for the second stack. This is explained by the negative pressure difference between the front and base of the first stack and a positive pressure difference for the second and third stack. Also seen is that the region and magnitude of the high pressure on the front face of the second stack, Figure 10, is larger for the cases with the voids. Finally, at the base of the trailer, the case without voids shows a lower

**FIGURE 16** Total pressure coefficient at  $y = 0$  at the windward side of the vehicle for L4.25\_D0.35\_RS0\_nSH, with and without the voids between the logs, at a 5° yaw. The main differences are at the front and base of each stack. The lower total pressure is seen in front of the first and third stack for the case with voids; however, a larger total pressure for the front of the second stack. Below, the cross-section of each stack is shown with the x-velocity inside the three stacks with voids. The first stack has a negative flow direction to the freestream flow, but the other two stacks have a positive flow direction.

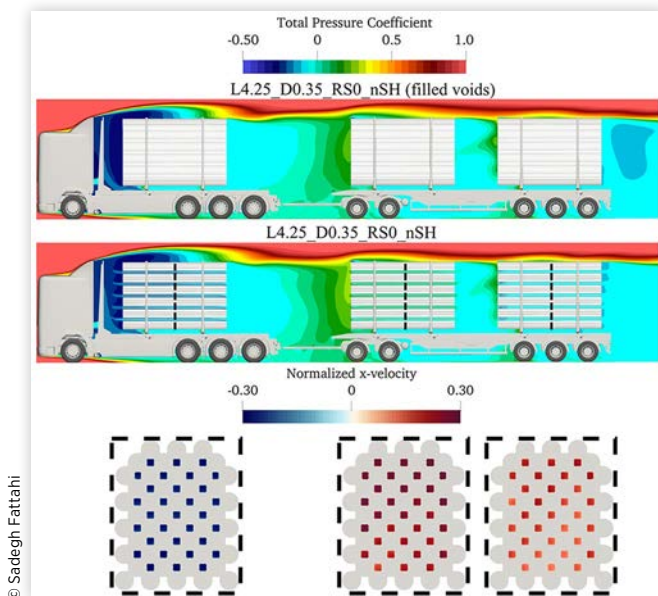
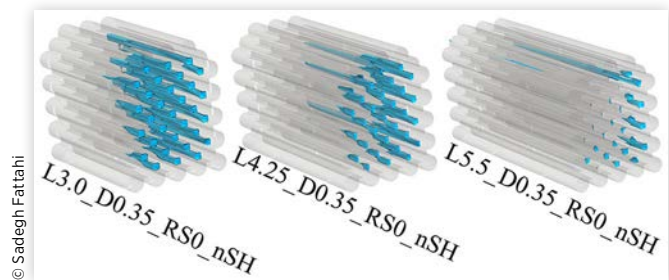


**FIGURE 17**  $C_{p_{tot}} = 0$  inside the voids of the third stack for the three different log lengths with  $D = 0.35$  at a 10° yaw. More pronounced separation is seen with short log lengths.



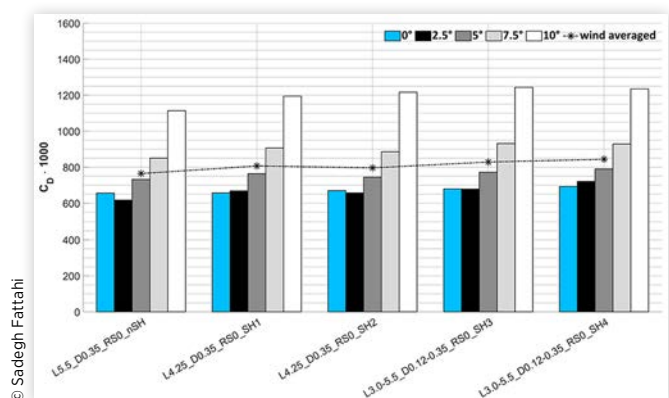
pressure in the wake, which is due to the absence of the voids to allow for flow through the stacks and evening out the pressure difference. Instead smaller low-pressure regions are present behind each individual log due to the flow exiting at the base of the vehicle through these voids and creating smaller recirculation regions. The results are presented for  $D = 0.35$  m; however, the same trend is seen for the other diameters.

The influence of the voids and the length of the logs is clear at a 10° yaw, Figure 17, as the voids and the shorter log lengths exhibit clear separation inside the voids, which is not seen to nearly the same level for  $L = 5.5$  m. This effect is due to the shorter log lengths allowing for more flow entrainment between the stack, as explained earlier and seen in Figure 12. This effect is also present at lower yaw angles, however to a lower extent. The increased drag count arising from these separations are 12, 33, and 55 for log lengths 5.5 m, 4.25 m, and 3 m, respectively. The longest log length of  $L = 5.5$  m has a much lower drag compared to the shorter log lengths.

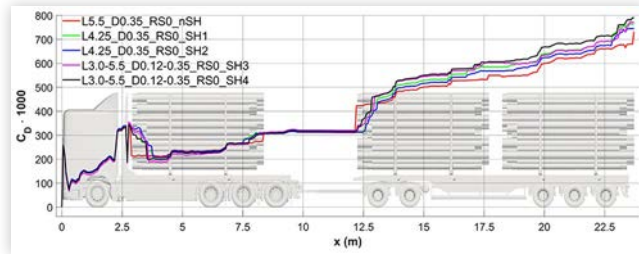
## Shuffle

The total drag and the wind averaged drag for the shuffled cases are seen in Figure 18, together with the theoretical baseline case (L5.5\_D0.35\_RS0\_nSH). The stacks used L4.25\_D0.35\_RS0\_SH1, L4.25\_D0.35\_RS0\_SH2, L3.0-5.5\_D0.12-0.35\_RS0\_SH3, and L3.0-5.5\_D0.12-0.35\_RS0\_SH4 correspond to

**FIGURE 18** The drag for the shuffled cases together with the theoretical baseline stack. The black line represents the wind averaged result for each case. Smaller differences are seen between the cases for the higher yaw angles.



**FIGURE 19** Drag accumulation along the truck for the different shuffled cases at a 5° yaw. The theoretical baseline case has the lowest drag and L3.0-5.5\_D0.12-0.35\_RS0\_SH4 has the highest, largest difference between the cases starting at the beginning of the second stack.



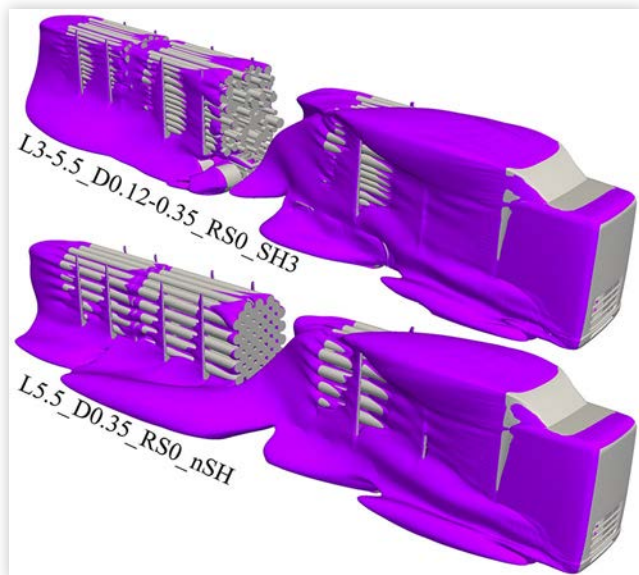
© Sadegh Fattahi

Figure 5. At all yaw angles, the shuffled cases have a higher drag compared to the theoretical baseline. This leads to a slightly higher wind averaged drag for the shuffled cases but still closest to a 5° yaw. The cases with the same log length and diameter, only shuffled (L4.25\_D0.35\_RS0\_SH1 and L4.25\_D0.35\_RS0\_SH2), show a close matching wind averaged drag, lower than the cases with randomized length and diameter (L3.0-5.5\_D0.12-0.35\_RS0\_SH3 and L3.0-5.5\_D0.12-0.35\_RS0\_SH4).

As Figure 19 shows, some differences in drag occur at the front face of the first stack, as the random nature of the stacking results in local separation regions. At the beginning of the second stack, all cases have similar total drag, but a significant difference occurs along the trailer.

Looking at Figure 20, it is seen that the surfaces at which  $C_{p_{tot}} = 0$  on the second and third stack differ, showing different

**FIGURE 20** Iso-surface of  $C_{p_{tot}} = 0$  for L3.0-5.5\_D0.12-0.35\_RS0\_SH3 and theoretical baseline case at a 5° yaw. The shuffled case shows large areas of  $C_{p_{tot}} = 0$  around the second and third stack, showcasing regions of energy loss. This is particularly visible on the side and beginning of the stacks. A larger wake is seen on the leeward side for the theoretical baseline case.

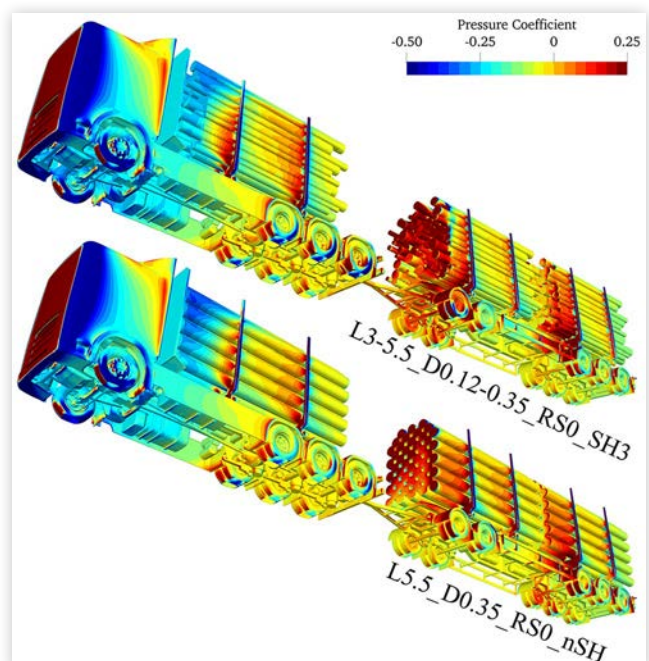


© Sadegh Fattahi

regions of energy loss along the logs. The shuffled stacks show larger regions of pressure loss on the sides of the stacks and along each protruding log, which is due to the random protrusion instead of a flat surface like the theoretical baseline stack. This protrusion of the logs leads to complex flow behavior at the front and rear faces of each stack, where each is protruding, deflecting, and redirecting the high-energy flow in different directions. This behavior is seen in all shuffled cases. The theoretical baseline stack shows a larger leeward side wake emanating from the base of the first stack extending to the end of the second stack, which is not present in the shuffled case. This is due to the reduced flow entrainment in the gap between the first and second stack, compared to the shuffled cases, creating a larger wake on the leeward side. Since the shuffled case has larger flow entrainment in the gap, thereby an acceleration of the flow, it results in a lower pressure on the windward side of the tractor wheels, Figure 21. The shuffled stacks cause significant pressure differences for the dolly wheels, wheel covers, and axles, Figure 21, with a larger downwash towards the underbody of the dolly and trailer. The differences are because the theoretical baseline case redirects the flow towards the sides and prevents large portions of high-energy flow from hitting those areas. Shuffles 1 and 2 are even more prone to this behavior due to their shorter lengths, thus a larger amount of high energy flow finding its way to the underbody and the wheels. The protrusions of each log do reduce the flow entrainment between the stacks described earlier for the shorter logs, Figure 12; however, that flow feature is still present, especially for Shuffles 1 and 2 since the logs are shorter compared to Shuffles 3 and 4.

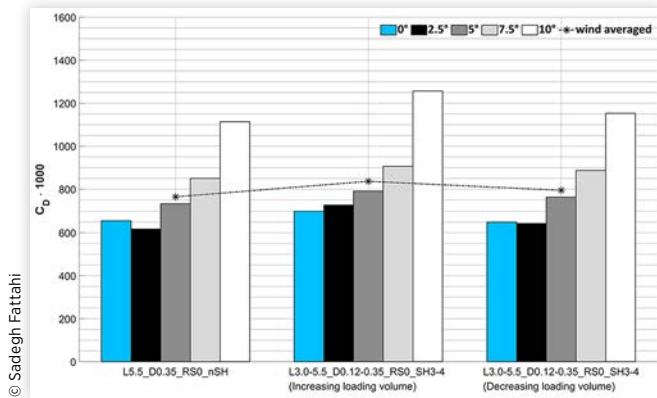
The other shuffled cases, as seen in the drag figure, exhibit similar behavior, however, at different points, due to the

**FIGURE 21** Pressure coefficient for L3.0-5.5\_D0.12-0.35\_RS0\_SH3 and the theoretical baseline case at a 5° yaw. The largest differences are seen at the dolly with higher pressure on the shuffled case. Also noticeable are the larger low-pressure regions on the windward wheels below the first stack.



© Sadegh Fattahi

**FIGURE 22** The drag for the increasing and decreasing loading volumes cases together with the theoretical baseline stack. The black line represents the wind averaged result for each case. The cases differ more at the higher and lower yaw angles.



random stacking nature of the logs. However, the larger flow features discussed above, for L3.0-5.5\_D0.12-0.35\_RS0\_SH3, are also present in other shuffled cases.

## Loading Volume

For the increasing loading volume, the drag is higher compared to the theoretical baseline case for all yaw angles, [Figure 22](#). However, the case with decreasing loading volume shows less of a difference to the theoretical baseline case for all yaw angles simulated. The wind averaged drag for the decreasing loading volume case is closer to the theoretical baseline case, 30 counts higher, while being 72 counts higher for the increasing loading volume.

There are some small differences in drag at the gap between the first stack and base of the cab, [Figure 23](#). This is due to the wake at the top, created by the separation at the deflector, which is slightly larger for the increasing loading volume case since the first stack is the smallest stack in this case. A similar drag is seen just upstream of the trailer, where larger differences of the drag arise from the loading volume. From there on, the accumulation of drag is higher for both the increasing and decreasing loading volume cases compared to the theoretical

**FIGURE 23** Drag accumulation along the truck for increasing and decreasing loading volume cases, together with the theoretical baseline case at a 10° yaw. The theoretical baseline case has the lowest drag and the increasing loading volume case has the largest. The main differences start at the front of the second stack.

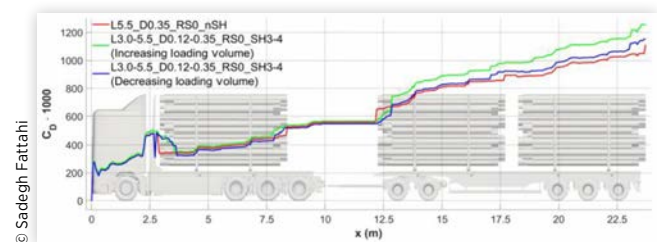
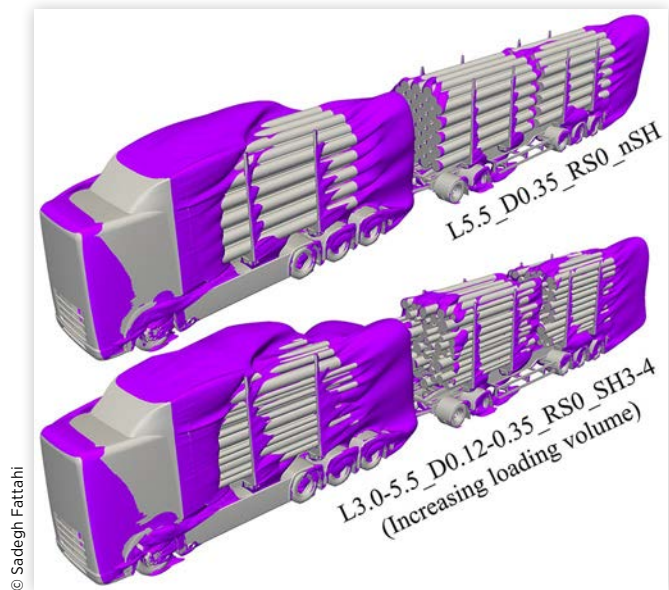
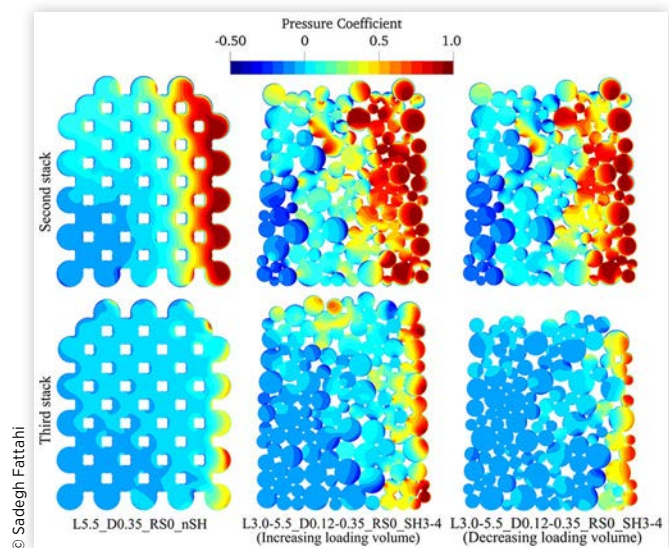


**FIGURE 24** Iso-surface of  $C_{p_{tot}} = 0$  for increasing loading volume case and theoretical baseline case at a 10° yaw. The increasing loading volume case shows large areas of  $C_{p_{tot}} = 0$  around the second and third stack, showcasing regions of pressure losses. The wake between the stacks and the base wake is slightly larger for the increasing loading volume case.



baseline case. These differences arise from the smaller separation regions along the second and third stack giving rise to smaller wakes contributing to the total drag, seen in [Figure 24](#). The same flow behavior is seen for the decreasing loading volume case. However, the larger drag of the increasing loading volume is due to more high-energy flow penetrating between the stack gaps, resulting in the larger pressure drag on the front surface of the second and third stack seen in [Figure 25](#). This is

**FIGURE 25** Pressure coefficient of the front face of the second and third stack at a 10° yaw with the right side being the windward side. The increasing loading volume case shows the largest area of high pressure compared to the other cases.



visible on the windward side of the stack. The increasing loading volume also exhibits high-pressure regions at the top of the front face of the third stack. This is due to the third stack having a larger surface area than the second stack since the high-energy flow is not deflected above the front face of the third stack. This behavior is present even in shuffled cases discussed previously; however it is almost completely absent when the loading volume is decreasing. At the end of the last stack for these cases, drag increases even further while the theoretical baseline case does not change much. This is due to the random protrusions of the stacks and not a distinct separation point for the entire stack, as in the theoretical baseline case, thus increasing the size of the base wake. The flow behaviors described are similar at lower yaw angles.

The change in loading volume, whether it is decreasing or increasing, does not show any larger case-specific flow feature attributed to any of them that is not already present in the shuffled cases. As seen in Figure 24, there are smaller local regions of separation along the stacks for the increasing loading volume case. This is similar to the features of the shuffled cases, however, that is associated with the random protrusions of the logs, which are not the case of the theoretical baseline.

## Formulation of Generic Stack

Based on the results presented for all the different stack variations including log length, diameter, surface roughness, shuffled stacks, and different loading volumes, a new generic stack is developed, which aims to be representative of a typical stack on the road and its aerodynamic properties. As concluded earlier the surface roughness of the stacks did not show any specific flow features associated with it, and neither does it show a significant impact on the drag, thus why the new generic stack will have smooth surfaces. Yet another reason for excluding the surface roughness is the added computational cost, since the logs require a finer mesh to resolve the geometry of the surface and thus an increased simulation cost.

The investigation of the log length showed a decrease in drag with increased log length, which is especially noticeable with the longest log, 5.5 m. The shorter log lengths of 3 m and 4.25 m both had similar flow features especially between the second and third stack, which is not present in the 5.5 m case. To include this effect, the new generic stack will consist of logs being 4.25 m long, which is also a mean value of the logs being transported on the road, which is more representative than the 3 m logs.

The change in diameter did not result in any flow features around the stacks but only a change of the front surface area of the stacks acting as a wall. Thus, the log diameter will remain the same as the theoretical baseline stack of 0.35 m for the new generic stack. This also results in a slightly reduced mesh size and less problematic regions, small voids between the stack, giving rise to divergence issues. Not including the voids, which is a more unrealistic case, does influence the drag as well as the behavior of the flow entrainment in different regions. These voids together with the shorter log lengths also

exhibit flow separation inside the voids, which is not present for  $L = 5.5$  m to the same extent. Thus, based on this, the voids are an important feature to include in the stacks.

The shuffling of the stacks does have an impact on the drag where the protrusion of the stacks gives rise to flow local low-pressure regions along the stacks especially at the front face of the stacks.

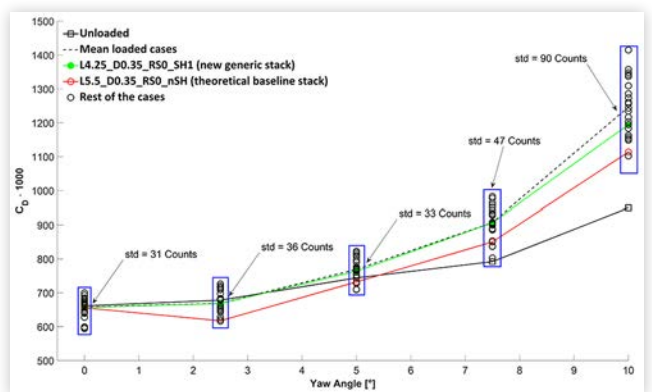
L3.0-5.5\_D0.12-0.35\_RS0\_SH3 and L3.0-5.5\_D0.12-0.35\_RS0\_SH4 where the logs are completely randomized did not show any larger difference to L4.25\_D0.35\_RS0\_SH1 and L4.25\_D0.35\_RS0\_SH2 where only shuffling of the same logs is done. The shuffled cases also exhibit a downwash towards the underbody of the trailer and dolly in front of the second stack, which contributes to pressure drag. Thus it is deemed necessary to include shuffling of the stack, but excluding complete randomized generation of logs size in each stack. These complete random stacks also come with added computational cost due to the more complex geometry and finer mesh needed to resolve the small voids between the logs. The shuffle included will be the same as the shuffle in L4.25\_D0.35\_RS0\_SH1 since none of them exhibited any case-specific flow features compared to each other.

As stated earlier, changing the loading volume, which effectively changes the stack height, did not exhibit any height-specific flow features, but the differences were mainly due to the protrusion of the logs, which is already modelled in the shuffled cases. The changes in flow behavior are of the same nature as the shuffled cases; thus having three different stacks with different heights is not deemed necessary to be included in the new generic stack.

Based on these findings, the new generic stack will be L4.25\_D0.35\_RS0\_SH1. This has all the characteristic flow features of all the stacks investigated, which can be used in future studies for improving the aerodynamic performance of the truck.

The drag for all simulated cases together with new generic and theoretical baseline stack, Figure 26, shows that the new generic stack is a better representation of the variations of the stack, compared to the theoretical baseline, as the drag is

**FIGURE 26** The drag for all cases investigated together with the theoretical baseline stack and new generic stack highlighted as red and green, respectively. The new generic stack shows a better average drag representation for each yaw angle.



similar to the mean of all stack configurations. It shows also how the drag is more spread between the cases with increased yaw angle, as shown by the standard deviation (std) for all cases at each angle. This shows that the new generic stack is a representative stack at all yaw angles investigated. The old stack shows a much lower drag for almost all yaw angles, resulting in a consistent underpredicted drag. As for all cases investigated, the drag at a 5° yaw was closest matching to the wind averaged drag. This new generic stack can thus be used in a reference configuration of a loaded timber truck, together with the unloaded vehicle, for further aerodynamic investigation and improvement of a timber truck at a 5° yaw.

## Conclusions

In this paper, an investigation is conducted by looking into the modelling of timber logs, for a loaded timber truck, and its influence on the aerodynamics of the vehicle using CFD. Different geometrical modifications are investigated such as surface roughness, log length, log diameter, voids between the logs, shuffling of the logs in the stack, and different loading volumes. It is found that shorter lengths, voids between the logs, and a certain degree of shuffling of the stacks created flow features that are not present in all cases and important to the aerodynamic behavior of the vehicle. Log diameter, surface roughness, and different loading volumes do not show any geometry-specific flow features, which are not present in the other cases.

The new generic stack exhibits flow features such as flow entrainment between the stacks influencing the extent of separation along the stacks, related to the log length; smaller separations on each individual log due to their individual protrusions, related to shuffling of the logs; and voids between the logs affecting the pressure difference between the front and base of the stack. Based on these, a generic stack is created representative of a realistic timber stack to be used for future aerodynamic investigation and optimization. The final outcome of this research results in a new baseline loaded truck where the three stacks used are identical to each other, and the new generic stack consists of logs with a length of 4.25 m, a diameter of 0.35, and a completely smooth surface, and finally, these logs are stacked with a certain degree of shuffling.

## Contact Information

### Sadegh Fattahi

Linköping University  
Applied Thermodynamics and Fluid Mechanics  
581 83 Linköping SWEDEN  
[sadegh.fattahi@liu.se](mailto:sadegh.fattahi@liu.se)

## Acknowledgments

This work is carried out within the ET-Taero2 project and the financial support by the Swedish Energy Agency is gratefully acknowledged. The Swedish National Infrastructure for Computing (SNIC) at National Supercomputer Centre at

Linköping University (NSC) is acknowledged for providing resources for the simulations performed.

## Definitions/Abbreviations

- $C_D$  - Drag coefficient
- $C_f$  - Skin friction coefficient
- $C_p$  - Pressure coefficient
- $C_{ptot}$  - Total pressure coefficient
- CFD - Computational fluid dynamics
- $D$  - Diameter of a log
- $H$  - Height of the stack
- $H_{truck}$  - Height of the truck body
- $L$  - Length of a log
- $L_{truck}$  - Length of the truck body
- $p$  - Pressure
- RKE - Realizable k-epsilon
- RS - Rough surface
- SH - Shuffle
- SS - Smooth surface
- $U$  - Velocity
- $U_{x\infty}$  - Freestream velocity in x
- $U_{y\infty}$  - Freestream velocity in y
- $U_\infty$  - Freestream velocity
- $W_{truck}$  - Width of the truck body
- $y^+$  - Dimensionless wall distance
- $\beta$  - Yaw angle
- $\rho_\infty$  - Density
- $\tau$  - Wall shear stress
- $\omega$  - Wheel angular velocity

## References

1. Hucho, W.-H., *Aerodynamics of Road Vehicles* (Warrendale, PA: Society of Automotive Engineers, Inc., 1998). ISBN:978-0-7680-0029-0.
2. Johannes, E., Ekman, P., Huge-Brodin, M., and Karlsson, M., "Sustainable Timber Transport—Economic Aspects of Aerodynamic Reconfiguration," *Sustainability* 2018:10, 1965, <https://doi.org/10.3390/su10061965>.
3. Ekman, P., Gårdhagen, R., Virdung, T., and Karlsson, M., "Aerodynamics of an Unloaded Timber Truck - A CFD Investigation," SAE Technical Paper 2016-01-8022, 2016, <https://doi.org/10.4271/2016-01-8022>.
4. Karlsson, M., Gårdhagen, R., Ekman, P., Söderblom, D. et al., "Aerodynamics of Timber Trucks - A Wind Tunnel Investigation," SAE Technical Paper 2015-01-1562, 2015, <https://doi.org/10.4271/2015-01-1562>.
5. Garner, G.J., "Wind Tunnel Tests of Devices for Reducing the Aerodynamic Drag of Logging Trucks," FERIC Technical Report TR-27, 1978.

6. von Hofsten, H., "Skogsbrukets transport- och arbetsfordon," Technical Report ARBETSRAPPORT 1003-2019, Skogforsk, 2019.
7. Cooper, K.R. and Leuschen, J., "Model and Full-Scale Wind Tunnel Tests of Second-Generation Aerodynamic Fuel Saving Devices for Tractor-Trailers," 2005.
8. Cooper, K.R., "Commercial Vehicle Aerodynamic Drag Reduction: Historical Perspective as a Guide," *The Aerodynamics of Heavy Vehicles: Trucks, Buses, and Trains* (Berlin: Springer, 2004), 9-28.
9. Anbarci, K., Acikgoz, B., Aslan, R., Arslan, O. et al., "Development of an Aerodynamic Analysis Methodology for Tractor-Trailer Class Heavy Commercial Vehicles," *SAE Int. J. Commer. Veh.* 6(2):441-452, 2013, <https://doi.org/10.4271/2013-01-2413>.
10. McAuliffe, B.R., "Improving the Aerodynamic Efficiency of Heavy Duty Vehicles: Wind Tunnel Test Results of Trailer-Based Drag-Reduction Technologies," NRC Report LTR-AL-2015-0272, National Research Council Canada, 2015.
11. Ekman, P., Gardhagen, R., Virdung, T., and Karlsson, M., "Aerodynamic Drag Reduction of a Light Truck - From Conceptual Design to Full Scale Road Tests," SAE Technical Paper 2016-01-1594, 2016, <https://doi.org/10.4271/2016-01-1594>.
12. SAE International Surface Vehicle Recommended Practice, "Guidelines for Aerodynamic Assessment of Medium and Heavy Commercial Ground Vehicles Using Computational Fluid Dynamics," SAE Standard J2966, Sept. 2013.
13. Shih, T.H., Liou, W.W., Shabbir, A., Yang, Z. et al., "A New k-Epsilon Eddy Viscosity Model for High Reynolds Number Turbulent Flows: Model Development and Validation," NASA Sti/recon Technical Report N, 95, 11442, 1994.
14. "ANSYS Fluent Theory Guide 19.2," ANSYS Inc., Canonsburg, PA, 2018.
15. Ekman, P., Gårdhagen, R., Virdung, T., and Karlsson, M., "Aerodynamic Drag Reduction - From Conceptual Design on a Simplified Generic Model to Full-Scale Road Tests," SAE Technical Paper 2015-01-1543, 2015, <https://doi.org/10.4271/2015-01-1543>.
16. Krastev, V. and Bella, G., "On the Steady and Unsteady Turbulence Modeling in Ground Vehicle Aerodynamic Design and Optimization," SAE Technical Paper 2011-24-0163, 2011, <https://doi.org/10.4271/2011-24-0163>.
17. Anbarci, K., Acikgoz, B., Aslan, R., Arslan, O. et al., "Development of an Aerodynamic Analysis Methodology for Tractor-Trailer Class Heavy Commercial Vehicles," *SAE Int. J. Commer. Veh.* 6(2):441-452, 2013, <https://doi.org/10.4271/2013-01-2413>.
18. SAE International, "SAE Wind Tunnel Test Procedure for Trucks and Buses," SAE Standard J2966, July 2012.
19. Johansson, S. and Gustavsson, M., "Investigation of Timber Vehicle Aerodynamics—Using CFD," Master's thesis, Linköping University, ISRN: LIU-IEI-TEK-A-19/03420—SE, 2019.
20. Surcel, M.-D., Provencher, Y., and Michaelsen, J., "Fuel Consumption Track Tests for Tractor-Trailer Fuel Saving Technologies," *SAE Int. J. Commer. Veh.* 2(2):191-202, 2009, <https://doi.org/10.4271/2009-01-2891>.